Infrared absorption of C H 3 S O 2 detected with time-resolved Fourier-transform spectroscopy

Li-Kang Chu and Yuan-Pern Lee

Citation: The Journal of Chemical Physics **124**, 244301 (2006); doi: 10.1063/1.2211610
View online: http://dx.doi.org/10.1063/1.2211610
View Table of Contents: http://scitation.aip.org/content/aip/journal/jcp/124/24?ver=pdfcov
Published by the AIP Publishing

Infrared absorption of CH_3SO_2 detected with time-resolved Fourier-transform spectroscopy

Li-Kang Chu
Department of Chemistry, National Tsing Hua University, 101, Section 2, Kuang Fu Road, Hsinchu 30013, Taiwan

Yuan-Pern Lee[a)]
Department of Applied Chemistry and Institute of Molecular Science, National Chiao Tung University, 1001 Ta-Hsueh Road, Hsinchu 30010, Taiwan; Institute of Atomic and Molecular Sciences, Academia Sinica, Taipei 10617, Taiwan

(Received 14 March 2006; accepted 15 May 2006; published online 23 June 2006)

A step-scan Fourier-transform spectrometer coupled with a 6.4 m multipass absorption cell was employed to detect time-resolved infrared absorption spectra of the reaction intermediate CH_3SO_2 radical, produced upon irradiation of a flowing gaseous mixture of CH_3I and SO_2 in CO_2 at 248 nm. Two transient bands with origins at 1280 and 1076 cm^{-1} were observed and are assigned to the SO_2-antisymmetric and SO_2-symmetric stretching modes of CH_3SO_2, respectively. Calculations with density-functional theory (B3LYP/aug-cc-pVTZ and B3P86/aug-cc-pVTZ) predicted the geometry, vibrational, and rotational parameters of CH_3SO_2 and CH_3OSO. Based on predicted rotational parameters, the simulated absorption band of the SO_2-antisymmetric stretching mode that is dominated by the *b*-type rotational structure agrees satisfactorily with experimental results. In addition, a band near 1159 cm^{-1} observed at a later period is tentatively attributed to CH_3SO_2I. The reaction kinetics of $CH_3+SO_2\rightarrow CH_3SO_2$ and $CH_3SO_2+I\rightarrow CH_3SO_2I$ based on the rise and decay of absorption bands of CH_3SO_2 and CH_3SO_2I agree satisfactorily with previous reports. © *2006 American Institute of Physics*. [DOI: 10.1063/1.2211610]

I. INTRODUCTION

Dimethyl sulfide (DMS, CH_3SCH_3) is the most abundant natural source of sulfur in the atmosphere.[1] The oxidation of DMS and other reduced sulfur compounds plays an important role not only in the formation of acid rain in the atmosphere but also in the formation of clouds; sulfate particles produced from these oxidation reactions may act as cloud condensation nuclei.[2] The methylsulfonyl radical (CH_3SO_2) has been proposed to be an important intermediate in the oxidation of reduced sulfur compounds in the atmosphere.[3–7] CH_3SO_2 might be produced either from reactions of CH_3SO with NO_2 and O_3,[4,5] or from isomerization of CH_3SOO that was formed via reaction of CH_3S with O_2 at low temperature.[8] CH_3SO_2 might also be formed in reactions of OH or O atoms with dimethyl sulfoxide[9,10] (DMSO). Chemically activated CH_3SO_2 might undergo prompt decomposition to form CH_3 and SO_2, or become thermalized before proceeding with further reactions.

In the condensed phase, an absorption band with maximum intensity in the range of 327–350 nm was ascribed to CH_3SO_2; the wavelength of the maximum depends on the solvent.[11,12] Electron paramagnetic resonance (EPR) spectra of CH_3SO_2, produced in solutions via reactions involving CH_3SO_2Cl,[13] photolysis of methylsulphinate ester, $CH_3S(O)OCH_3$, and di-*t*-butyl peroxide,[14] or photoisomerization of CH_3SOO have been reported;[15] observed spectra and calculations according to the semiempirical intermediate neglect of differential overlap (INDO) model indicate that this radical has a σ-type structure with the unpaired electron localized on the SO_2 moiety.[16]

In the gaseous phase, both methylsulfonyl radical (CH_3SO_2) and methoxysulfinyl radical (CH_3OSO) were produced with femtosecond collisional electron transfer and detected with variable-time neutralization-reionization mass spectrometry,[17] but gaseous CH_3SO_2 or CH_3OSO has never been spectrally characterized. Hence it is desirable to develop a detection technique to investigate the spectroscopy and reaction kinetics of gaseous CH_3SO_2 or CH_3OSO.

Several theoretical calculations have been performed to predict the energy, geometry, and vibrational wave numbers of CH_3SO_2 and CH_3OSO.[4,17–21] Two conformers of CH_3OSO are stable; *syn*-CH_3OSO is more stable than *anti*-CH_3OSO by ~8 kJ mol^{-1} which is more stable than CH_3SO_2 by ~13 kJ mol^{-1}.[17] According to calculations, reactions of CH_3 with SO_2 might proceed via three paths: a nearly barrierless channel to produce CH_3SO_2 and two channels with barriers ~80 kJ mol^{-1} to produce *anti*-CH_3OSO and *syn*-CH_3OSO; *anti*-CH_3OSO might readily transform to the more stable *syn*-CH_3OSO with a near-zero barrier, as shown in Fig. 1. Reaction of CH_3 with SO_2 is thus expected to be an effective method to produce CH_3SO_2 for laboratory investigations.

We have demonstrated that, by coupling a step-scan Fourier-transform infrared (FTIR) spectrometer with a multipass absorption cell, time-resolved infrared absorption

[a)]Author to whom correspondence should be addressed. Electronic mail: yplee@mail.nctu.edu.tw

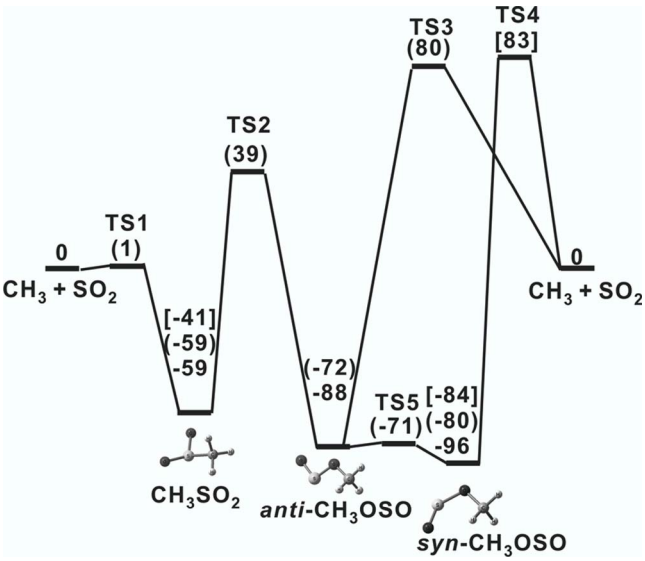

FIG. 1. Potential energy diagram for the reaction of CH_3 with SO_2. Relative energies of isomers of CH_3SO_2 calculated with B3LYP/aug-cc-pVTZ in this work are listed. Energies calculated with the G2(MP2) method in Ref. 17 are listed in parentheses. Energies calculated with the PMP4SDTQ method in Ref. 19 are listed in brackets.

spectra of gaseous reaction intermediates such as ClCO (Ref. 22) and ClSO (Ref. 23) and species in vibrationally excited states (HCl^*, CH_4^*) were recorded.[24,25] Here we report an application of a step-scan FTIR spectrometer to record time-resolved infrared absorption spectra of the intermediate CH_3SO_2 from reactions of CH_3 with SO_2.

II. EXPERIMENTS

A White cell with a volume of ~1600 cm^3 and an effective path length of 6.4 m (base path of 20 cm) serves as the reactor. The housing of the White cell has two rectangular (3×12 cm^2) quartz windows on the sides to pass the photolysis laser beam that propagates perpendicular to multipassing IR beams. The laser beam is multiply reflected between a pair of external rectangular laser mirrors and passes these quartz windows and the White cell after each reflection. A KrF excimer laser (GAM Laser, EX100H/60) operated at 7 Hz with typical output energy of ~100 mJ $pulse^{-1}$ at 248 nm and a beam expanded by a telescope to a dimension $\sim4\times1.2$ cm^2 was employed for photodissociation. The White cell was placed in the sample compartment of the FTIR spectrometer. A commercial step-scan spectrometer (Thermo Nicolet, Nexus 870) equipped with a fast mercury cadmium telluride (MCT) detector (20 MHz) and an external 14 bit digitizer (Gage Applied Technology, CompuScope 14 100, 10^8 sample s^{-1}) was employed for data acquisition. The position of the moving mirror of FTIR was maintained to within ±0.2 nm at each step in the step-scan mode.[26]

Techniques for obtaining time-resolved difference absorption spectra with a step-scan FTIR spectrometer are well established.[24,27] After preamplification, the ac-coupled signal from the MCT detector was further amplified (Stanford Research Systems, Model SR560) 20 times with a bandwidth 100–1 M Hz before being sent to the external 14 bit digitizer, whereas the dc-coupled signal was sent directly to the internal 16 bit digitizer (2×10^5 sample s^{-1}) of the spectrometer. Typically, 300 data points were acquired at 1 μs integrated intervals (100 dwells at 10 ns gate width) after each laser shot; the signal was typically averaged over 16 laser shots at each scan step. We utilized undersampling to decrease the number of points in the interferogram, hence the duration of data acquisition, by employing proper optical filters to define a small spectral region. For spectra in the range of 1580–835 cm^{-1} at a resolution of 2.0 cm^{-1}, 960 scan steps were required, and the data acquisition took ~60 min. To improve further the ratio of signal to noise, we recorded and averaged ten sets of data under similar experimental conditions.

A flowing mixture of $CH_3I/SO_2/CO_2$ with flow rates $F_{CH_3I}\cong0.10$, $F_{SO_2}\cong0.34$, $F_{CO_2}\cong20.4$ SCCS (SCCS denotes cubic centimeter per second at STP), and total pressure $P_T=297$ Torr at 298 K was irradiated at 248 nm. The efficiency of photolysis of CH_3I is estimated to be 2% based on its absorption cross section $\sim8\times10^{-19}$ cm^2 $molecule^{-1}$ at 248 nm.[28]

CH_3I (99%, Riedel–de Haën) and SO_2 (99.9%, Matheson) were used without further purification. CO_2 (99.99%) was purified by passing it through a trap at 218 K.

III. THEORETICAL CALCULATIONS

We employed the GAUSSIAN 03 program to calculate the energy, equilibrium geometry, harmonic wave numbers, and IR intensities of CH_3SO_2 and CH_3OSO with B3LYP and B3P86 density-functional theories.[29] The B3LYP method uses Becke's three-parameter hybrid exchange functional with a correlation functional of Lee *et al.*[30,31] The B3P86 method uses Becke's three-parameter hybrid exchange functional with Perdew's gradient-corrected correlation functional.[32] Dunning's correlation-consistent polarized-valence triple-zeta basis sets, augmented with *s*, *p*, *d*, and *f* functions (aug-cc-pVTZ) (Refs. 33 and 34), was applied in all calculations except those for CH_3SO_2X (X=F, Cl, Br, and I), in which standard 3-21G* basis sets were employed. All reported energies include vibrational zero-point energy. Analytic first derivatives were utilized in geometry optimization, and harmonic vibrational wave numbers were calculated analytically at each stationary point.

The geometries of CH_3SO_2 and two conformers of CH_3OSO calculated with B3P86/aug-cc-pVTZ are shown in Fig. 2; those calculated with B3LYP are similar and are listed parenthetically. The most stable species is *syn*-CH_3OSO with the terminal O atom on the same side as the methyl group; the S=O bond length of 1.481 Å is greater than the experimental value of 1.432 Å of SO_2,[35] and the S–O bond length of 1.638 Å is greater than the value of 1.481 Å of SO.[36] Similar to previous report using G2(MP2)/6-31+G(2*d*,*p*),[17] *anti*-CH_3OSO has energy of 8 kJ mol^{-1} greater than *syn*-CH_3OSO. Its S=O bond is slightly shorter, whereas its S–O bond is slightly longer than those of *syn*-CH_3OSO, as indicated in Figs. 2(B) and 2(C).

CH_3SO_2 is greater in energy than *syn*-CH_3SO_2 by 28 kJ mol^{-1} (B3P86) or 37 kJ mol^{-1} (B3LYP); a previous calculation based on the G2(MP2)/6-31+G(2*d*,*p*) method

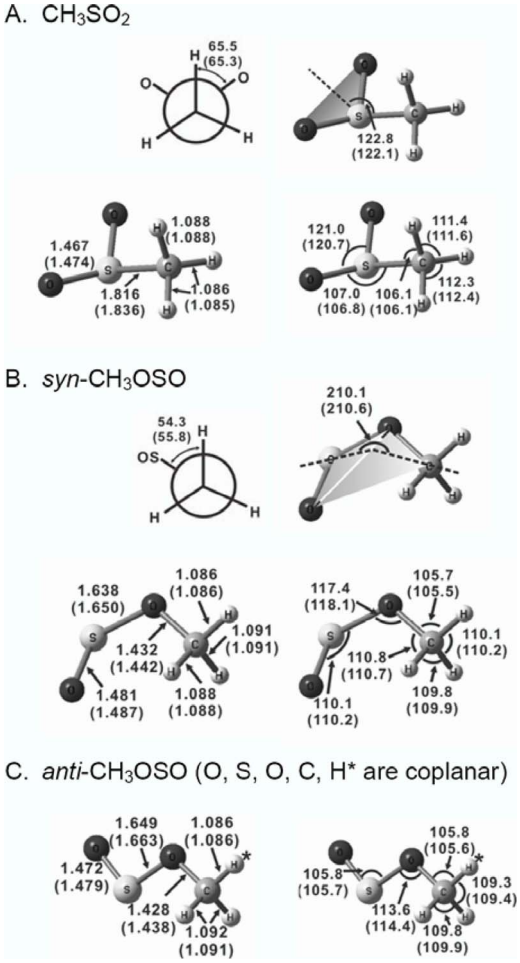

FIG. 2. Geometries predicted with B3P86/aug-cc-pVTZ and B3LYP/aug-cc-pVTZ methods for CH_3SO_2 (A), *syn*-CH_3OSO (B), and *anti*-CH_3OSO (C). Bond lengths are in Å and bond angles are in degrees. Results from B3LYP are listed parenthetically.

yielded 21 kJ mol^{-1}.[17] The C–S bond length of 1.816 Å predicted with B3P86/aug-cc-pVTZ in this work [Fig. 2(A)] is similar to the value of 1.818 Å of CH_3SH.[37] The predicted S═O bond length of 1.467 Å is slightly greater than the experimental value of 1.432 Å for SO_2 (Ref. 35) and the value of 1.450 Å predicted for $ClSO_2$.[38] Previous reports using smaller basis sets yielded similar results[17,19] except that from UHF/6-31G(*d*),[20] which predicted two eclipsed C–H and S–O bonds rather than staggered C–H and S–O bonds.

Vibrational wave numbers and IR intensities of CH_3SO_2, *anti*-CH_3OSO, and *syn*-CH_3OSO predicted with B3LYP and B3P86 methods are compared in Table I. The two most intense bands of CH_3SO_2 predicted with B3P86 (B3LYP) methods are at 1262 (1223) and 1074 (1044) cm^{-1}, corresponding to the SO_2-antisymmetric and SO_2-symmetric stretching modes, respectively. Previous calculations using B3LYP/6-31+G(2*d*,*p*) yielded 1208 and 1021 cm^{-1}, respectively.[17]

The wave numbers of the most intense bands of *syn*-CH_3OSO predicted with B3P86 (B3LYP) methods are 717 (690), 1028 (995), 1162 (1136), 1166 (1165), and 3046 (3036) cm^{-1}, corresponding to S–O stretching, C–O stretching, S═O stretching mixed with CH_3 wagging, S═O stretching mixed with CH_3 rocking, and CH_3-symmetric stretching modes, respectively. Previous calculations using B3LYP/6-31+G(2*d*,*p*) yielded 663, 989, 1105, 1165, and 3038 cm^{-1}, respectively.[17]

The wave numbers of the most intense bands of *anti*-CH_3OSO predicted with B3P86 (B3LYP) methods are 742 (715), 1046 (1014), 1195 (1167), and 3031 (3022) cm^{-1}, corresponding to S–O stretching, C–O stretching, S═O stretching, and CH_3-symmetric stretching modes, respectively. Pre-

TABLE I. Comparison of energies, harmonic vibrational wave numbers, and IR intensities (listed in parentheses) of CH_3SO_2, *syn*-CH_3OSO, and *anti*-CH_3OSO calculated with B3LYP and B3P86/aug-cc-pVTZ methods.

CH_3SO_2				*syn*-CH_3OSO				*anti*-CH_3OSO			
B3LYP		B3P86		B3LYP		B3P86		B3LYP		B3P86	
Energy[a]/hartree+588											
−0.555714		−1.301023		−0.569881		−1.311672		−0.566647		−1.308466	
Vibrational wave numbers/cm^{-1} (IR intensities/km mol^{-1})											
163	(0)	165	(0)	73	(7)	75	(7)	45	(0)	46	(0)
293	(0)	296	(0)	123	(3)	121	(3)	107	(2)	102	(2)
368	(21)	374	(21)	250	(9)	254	(10)	242	(0)	241	(0)
445	(16)	452	(16)	479	(5)	486	(5)	414	(2)	420	(2)
612	(15)	644	(15)	690	(103)	717	(103)	715	(133)	742	(132)
932	(6)	928	(7)	995	(181)	1028	(176)	1014	(186)	1046	(184)
949	(0)	946	(0)	1136	(73)	1162	(33)	1167	(80)	1168	(1)
1044	(60)	1074	(62)	1165	(3)	1166	(36)	1168	(1)	1185	(8)
1223	(125)	1262	(134)	1181	(4)	1181	(12)	1185	(6)	1195	(82)
1304	(1)	1297	(1)	1461	(1)	1455	(1)	1467	(1)	1460	(1)
1446	(6)	1437	(5)	1486	(9)	1479	(10)	1493	(9)	1486	(10)
1453	(10)	1444	(11)	1502	(11)	1497	(12)	1500	(14)	1494	(16)
3061	(0)	3071	(0)	3036	(35)	3046	(34)	3022	(48)	3031	(46)
3165	(1)	3181	(1)	3114	(16)	3129	(15)	3084	(26)	3100	(23)
3182	(0)	3200	(0)	3146	(6)	3163	(5)	3138	(6)	3156	(5)

[a]Vibrational zero-energy included.

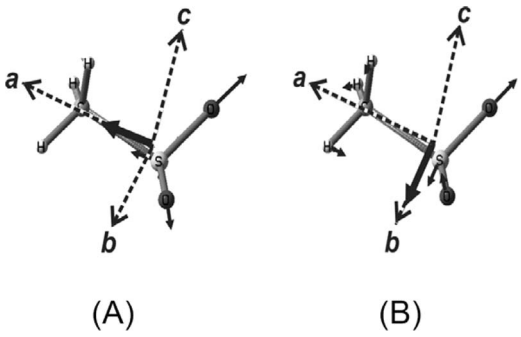

FIG. 3. Displacement vectors (thin arrows) and vector of dipole derivatives (bold arrows) predicted with the B3P86/aug-cc-pVTZ method for SO_2-symmetric stretching (A) and SO_2-antisymmetric stretching modes (B) of CH_3SO_2. Rotational axes *a*, *b*, and *c* are also shown as arrows with dashed lines.

vious calculations using B3LYP/6-31+G(2*d*,*p*) yielded 689, 1008, 1185, and 3023 cm^{-1}, respectively.[17]

Predicted displacement vectors (thin arrows) for the SO_2-symmetric and SO_2-antisymmetric stretching modes of CH_3SO_2 and the associated dipole derivatives (thick arrows) are shown in Figs. 3(A) and 3(B), respectively. The three rotational axes *a*, *b*, and *c* of CH_3SO_2 are also indicated in Fig. 3 as arrows with dashed lines.

Rotational parameters predicted with B3P86 and B3LYP for the ground state and states vibrationally excited in the SO_2-symmetric stretching and SO_2-antisymmetric stretching modes of CH_3SO_2 are listed in Table II for comparison. The difference in predicted geometries using B3LYP and B3P86 results in variations less than 1.9% for rotational parameters of both the ground and the excited states.

IV. EXPERIMENTAL RESULTS AND DISCUSSION

A. Photolysis of the mixture $CH_3I/SO_2/CO_2$

Because the precursors became highly internally excited upon laser irradiation, we added excessive CO_2 to thermalize species in the system; absorption of the internally hot parent molecules typically yields upward-pointing features on each side of the downward parent band in the difference absorption spectra, thus interfering with observation of nearby absorption features of the species of interest.[23] The excess energy of a reaction adduct might also facilitate decomposition, thus hampering its observation.

A representative three-dimensional plot of temporally and spectrally resolved spectra at 10 μs intervals upon laser irradiation at 248 nm of a flowing mixture of 297 Torr of $CH_3I/SO_2/CO_2$ (1.0/3.3/200) is shown in Fig. 4(A). In these difference spectra, signals pointing upward indicate production, whereas those pointing downward indicate a decrease in concentration. The consumption of CH_3I and SO_2 is shown as downward features near 1265, 1235, and 1160 cm^{-1}, respectively. An intense feature near 1280 cm^{-1} and a weak feature near 1076 cm^{-1} appeared after irradiation; they increased in intensity, reached maxima near 50 μs, and decayed afterwards. A band near 1160 cm^{-1} appeared at a later stage of reaction and became prominent after 150 μs. Spectra integrated over various reaction periods are represented in Fig. 4(B). The rise and decay of features near 1280 and 1076 cm^{-1} (marked A1 and A2, respectively), and the rise of the feature near 1160 cm^{-1} (marked B1) are clearly illustrated.

The spectra integrated over 20–80 μs intervals in the spectral region of 1000–1500 cm^{-1} are shown in trace (A) of Fig. 5; the spectral region of 1310–1390 is unusable due to saturated absorption of SO_2. The two new features at 1280 and 1076 cm^{-1} are marked as A1 and A2. Because part of the A1 band was subject to interference by weak absorption in the *R* branch of CH_3I near 1265 cm^{-1}, which decreases slightly upon photolysis, the A1 band appears narrower than its original form. The background spectrum of the flowing mixture is shown in trace (B) of Fig. 5, in which absorption due to CH_3I near 1250 cm^{-1} is marked; the downward band near 1240 cm^{-1} in Fig. 5(A) clearly matches the *P* branch of CH_3I. We corrected for this interference by spectral stripping; the spectrum in Fig. 5(B) was scaled and added to the spectrum in Fig. 5(A) in such a way that the *P*-branch region of CH_3I, 1250–1220 cm^{-1}, became nearly flat. The resultant

TABLE II. Comparison of rotational parameters of CH_3SO_2 in ground and vibrationally excited states calculated with B3LYP and B3P86/aug-cc-pVTZ.

Parameters		B3LYP/aug-cc-pVTZ	B3P86/aug-cc-pVTZ
Equilibrium	A/cm^{-1}	0.2817	0.2843
	B/cm^{-1}	0.2564	0.2608
	C/cm^{-1}	0.1475	0.1493
$v=0$	A/cm^{-1}	0.2808	0.2834
	B/cm^{-1}	0.2536	0.2583
	C/cm^{-1}	0.1463	0.1481
SO_2-symmetric stretching ($v=1$)	A/cm^{-1}	0.2793	0.2819
	B/cm^{-1}	0.2538	0.2585
	C/cm^{-1}	0.1459	0.1478
SO_2-antisymmetric stretching ($v=1$)	A/cm^{-1}	0.2795	0.2822
	B/cm^{-1}	0.2532	0.2579
	C/cm^{-1}	0.1460	0.1479

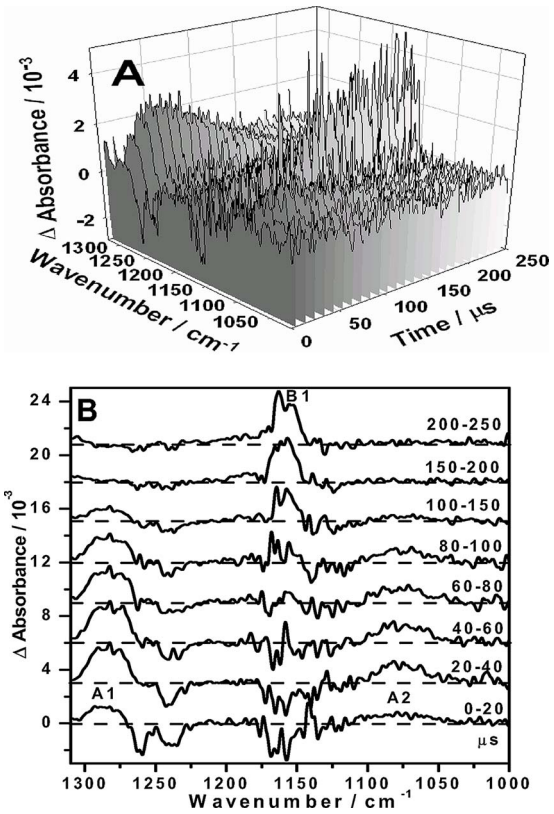

FIG. 4. (A) Three-dimensional plot of time-resolved difference absorption spectra upon laser photolysis (248 nm, 7 Hz, 21 mJ cm^{-2}) of a flowing mixture of $CH_3I/SO_2/CO_2$ (1.0/3.3/200) at 297 Torr and 298 K. The path length is 6.4 m and the resolution is 2.0 cm^{-1}. (B) Spectra integrated for various periods. Downward features are due to destruction of precursors CH_3I (1265 and 1235 cm^{-1}) and SO_2 (1160 cm^{-1}), whereas upward features A1 and A2 correspond to formation of CH_3SO_2 and the upward feature B1 corresponds to formation of CH_3SO_2I.

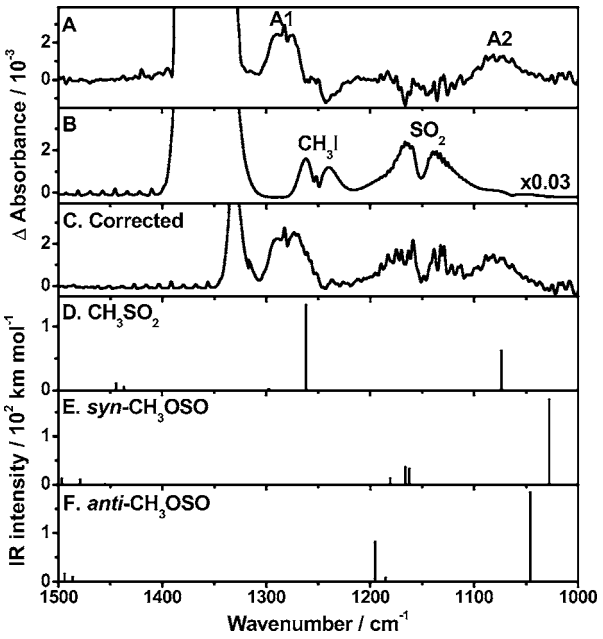

FIG. 5. (A) Transient difference absorption spectrum recorded upon 248 nm photolysis of a flowing mixture of $CH_3I/SO_2/CO_2$ (1.0/3.3/200) at 297 Torr and 298 K; resolution is 2 cm^{-1} and average period is 20–80 μs. New features are marked as A1 and A2. (B) The background absorption spectrum of the flowing mixture before photolysis. (C) The transient spectrum in (A) corrected for interference due to loss of parent molecules; see text. (D)–(F) Stick spectra of CH_3SO_2, *syn*-CH_3OSO, and *anti*-CH_3OSO, respectively, based on harmonic vibrational wave numbers and IR intensities predicted with the B3P86/aug-cc-pVTZ method.

spectrum is shown in trace (C) of Fig. 5; this corrected spectrum of the A1 band is used for comparison with spectral simulation.

B. Assignment of CH_3SO_2 absorption

The major product on photolysis of CH_3I at 248 nm is CH_3;[39] further reaction of CH_3 with SO_2 might form CH_3SO_2 or CH_3OSO. SO_2 has a small absorption cross section $\sim 9\times 10^{-20}$ cm^2 at 248 nm;[40] but it does not dissociate because the photodissociation threshold is $\sim$220 nm.[41] Considering that observed transient absorption features near 1280 and 1076 cm^{-1} (A1 and A2 bands) have vibrational wave numbers similar to observed values of 1309.6 and 1098.2 cm^{-1} for the SO_2-antisymmetric and SO_2-symmetric stretching modes of $ClSO_2$ isolated in solid Ar, respectively,[38] but smaller than values of 1361.8 and 1151.4 cm^{-1} for SO_2,[42] we believe that they are due to CH_3SO_2 rather than to CH_3OSO. The latter is expected to have a spectral pattern distinct from the SO_2-symmetric and SO_2-antisymmetric stretching modes.

Quantum-chemical calculations in this work provide further support for the assignment. IR absorption spectra in the region of 1000–1500 cm^{-1} predicted for CH_3SO_2, *syn*-CH_3OSO, and *anti*-CH_3OSO with B3P86/aug-cc-pVTZ are shown as stick diagrams in traces (D)–(F) of Fig. 5, respectively; predicted intensities are represented by the height of the sticks. Two most intense bands predicted at 1262 and 1074 cm^{-1} for CH_3SO_2 (without scaling) fit satisfactorily with experiments, with deviations of −1.4% and 0.2%, respectively. For comparison, previous predictions of vibrational wave numbers for the SO_2-antisymmetric and SO_2-symmetric stretching modes of $ClSO_2$ are within 1% (B3P86) and 2.8% (B3LYP) of experimental values from the matrix experiment.[38] The pattern of three intense bands predicted for *syn*-CH_3OSO at 1028, 1162, and 1166 cm^{-1} in this spectral region and two intense bands predicted for *anti*-CH_3OSO at 1046 and 1195 cm^{-1} are appreciably different from our observation.

The direction of the dipole derivative for the SO_2-antisymmetric stretching mode and the three principal rotational axes of CH_3SO_2 shown in Fig. 3(B) indicates that the associated rotational structure for this vibrational mode is mainly *b*-type, whereas that for the SO_2-symmetric stretching mode is mainly *a*-type [Fig. 3(A)].

As derivation of rotational parameters from observed spectra is unlikely with the present spectral resolution, we simulate the band contour to compare with observed spectra. The spectrum of SO_2-antisymmetric stretching band was simulated with the SPECVIEW program[43] using rotational parameters *A*, *B*, and *C* derived from B3P86/aug-cc-pVTZ calculations, $J_{max}=100$, $T=300$ K, and a Doppler line shape with full width at half maximum (FWHM)=2.0 cm^{-1}. Although rotational parameters predicted with B3P86 differ by 1.9% from those predicted with B3LYP, the ratios of rotational parameters of the upper ($v=1$) and the lower ($v=0$)

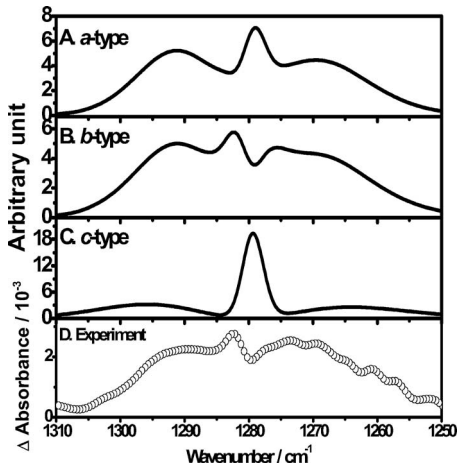

FIG. 6. Comparison of simulated and observed spectra of the SO_2-antisymmetric stretching mode of CH_3SO_2. Parameters employed in the simulation are $T=300$ K, $J_{max}=100$, $\nu_0=1280.1$ cm^{-1}, $A''=0.2834$ cm^{-1}, $B''=0.2583$ cm^{-1}, $C''=0.1481$ cm^{-1}, $A'=0.2822$ cm^{-1}, $B'=0.2579$ cm^{-1}, and $C'=0.1479$ cm^{-1}. (A) *a*-type component. (B) *b*-type component. (C) *c*-type component. (D) Corrected experimental observation shown in trace (C) of Fig. 5; the transition is expected to have mainly a *b*-type component.

states are nearly identical for both methods. Simulated *a*-, *b*-, and *c*-type spectra are shown in traces (A)–(C) of Fig. 6, respectively. The experimental observation shown in trace (D) of Fig. 6 agrees satisfactorily with the *b*-type contour [trace (B) of Fig. 6]; this agreement further supports our assignment of this band to the SO_2-antisymmetric stretching mode of CH_3SO_2. Keeping values $A''=0.2834$ cm^{-1}, $B''=0.2583$ cm^{-1}, $C''=0.1481$ cm^{-1} for $v=0$ and $A'=0.2822$ cm^{-1}, $B'=0.2579$ cm^{-1}, $C'=0.1479$ cm^{-1} for $v=1$ of the SO_2-antisymmetric stretching mode of CH_3SO_2 (Table II) unaltered in the simulation, a value $\nu_0=1280.1$ cm^{-1} was thus derived. Fitting of the SO_2-symmetric stretching band was not performed because of its unsatisfactory quality.

C. Possible formation of CH_3SO_2I

At a later stage of reaction, 100 μs after photolysis of the flowing mixture of $CH_3I/SO_2/CO_2$, a new feature near 1159 cm^{-1} appeared, as marked B1 in Fig. 4(B). The rise of this feature was accompanied by the decay of CH_3SO_2, indicating that this feature might be due to secondary reactions of CH_3SO_2. Because photolysis of SO_2 at 248 nm is negligible,[41] the major species upon photolysis of the mixture are expected to be CH_3, I, and SO_2. Two likely products of possible secondary reactions are therefore CH_3SO_2I and $(CH_3)_2SO_2$.

Vibrational wave numbers for the SO_2-symmetric and SO_2-antisymmetric stretching modes of $(CH_3)_2SO_2$ were reported to be 1162 and 1354 cm^{-1}, respectively.[44] The former fits satisfactorily with our observation and the latter was interfered with by absorption of SO_2 in our experiments. Vibrational wave numbers of CH_3SO_2I are unreported, but wave numbers of the SO_2-symmetric stretching bands of CH_3SO_2F, CH_3SO_2Cl, and CH_3SO_2Br were reported to be 1223, 1190, and 1178 cm^{-1}, respectively,[45,46] as listed in Table III.

Harmonic vibrational wave numbers for the SO_2-stretching modes of CH_3SO_2X (X=F, Cl, Br, and I), $CH_3SO_2CH_3$, and CH_3SO_2 predicted with B3P86/3-21G* are compared with experimental results in Table III. Using the ratios of observed to calculated values for CH_3SO_2X (X=F, Cl, and Br), we estimated that the SO_2-symmetric stretching mode of CH_3SO_2I should lie in the region of 1146–1167 cm^{-1}, similar to that of $(CH_3)_2SO_2$. Hence, identifying the carrier of the B1 band by vibrational wave numbers alone is ambiguous.

The disparate masses of $(CH_3)_2SO_2$ and CH_3SO_2I imply distinctive rotational parameters for these molecules; the former is much lighter, hence should have a bandwidth much greater than that of the much heavier CH_3SO_2I. Trace (A) of Fig. 7 shows a spectrum (1090–1220 cm^{-1}) integrated for the period of 150–250 μs after photolysis. Trace (B) of Fig. 7 is a simulated SO_2-symmetric stretching band of CH_3SO_2I using rotational parameters predicted with B3P86/3-21G*. The molecular parameters of CH_3SO_2I used for simulation are $J_{max}=100$, $T=300$ K, a Doppler line shape with FWHM=2.0 cm^{-1}, $A'=0.148\,52$, $B'=0.039\,24$, $C'=0.038\,77$, $A''=0.148\,89$ cm^{-1}, $B''=0.039\,29$ cm^{-1}, $C''=0.038\,79$ cm^{-1}, and $\nu_0=1159$ cm^{-1}. According to the calculated vector of the dipole derivative, the *b*-type structure dominates. Trace (C) of Fig. 7 shows an experimental spectrum of $(CH_3)_2SO_2$ in the 1190–1120 cm^{-1} region.[44] Our experimental result fits satisfactorily with the simulated spectrum of CH_3SO_2I, whereas the absorption band of $(CH_3)_2SO_2$ shows a much greater width than our observed

TABLE III. Comparison of SO_2-antisymmetric and SO_2-symmetric stretching wave numbers (in cm^{-1}) of CH_3SO_2X (X=F, Cl, Br, and I), $(CH_3)_2SO_2$, and CH_3SO_2 derived from B3P86/3-21G* calculations and from experiments.

	Calc.		Expt.		
	SO_2-antisymmetric stretching	SO_2-symmetric stretching	SO_2-antisymmetric stretching	SO_2-symmetric stretching	Reference
CH_3SO_2F	1462	1236	1415 (0.968)[a]	1223 (0.989)[a]	45
CH_3SO_2Cl	1427	1181	1401 (0.982)	1190 (1.008)	45
CH_3SO_2Br	1414	1174	1391 (0.984)	1178 (1.003)	45 and 46
CH_3SO_2I	1401	1158		1159 (1.001)	This work
$(CH_3)_2SO_2$	1398	1182	1356 (0.970)	1165 (0.986)	44
CH_3SO_2	1230	1035	1280 (1.041)	1076 (1.040)	This work

[a]Ratios of experimental to calculated vibrational wave numbers are listed in parentheses.

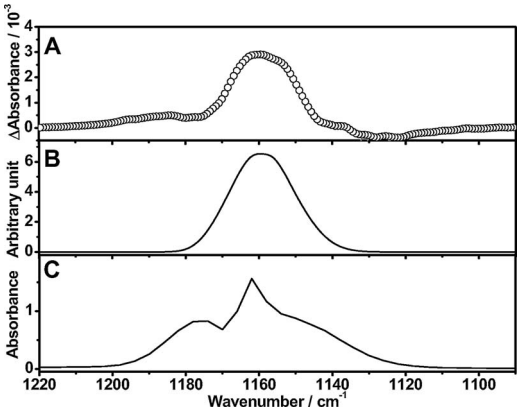

FIG. 7. Comparison of simulated and observed spectra of the SO_2-symmetric stretching mode of CH_3SO_2I. (A) Experimental observation integrated for period of 150–250 μs from spectra in Fig. 4(A). (B) Simulated spectrum of CH_3SO_2I with only the *b*-type component; rotational parameters are described in the text. (C) A previously reported spectrum of $(CH_3)_2SO_2$ (Ref. 44) in the region of 1090–1220 cm^{-1}. The transient absorption band in (A) fits better with the simulated spectrum of CH_3SO_2I in (B).

value. The B1 band near 1159 cm^{-1} is hence tentatively assigned to the SO_2-symmetric stretching mode of CH_3SO_2I.

D. Reaction kinetics of CH_3SO_2

As can be seen from the three-dimensional plot of Fig. 4(A), the intensity of the new feature near 1280 cm^{-1} (A1 band) increases initially, reaches its maximum near 50 μs, then decays with time. The temporal profile of the A1 band of CH_3SO_2, integrated over 1280–1300 cm^{-1}, is shown in Fig. 8(A). Fitting the temporal profile of CH_3SO_2 to a simple

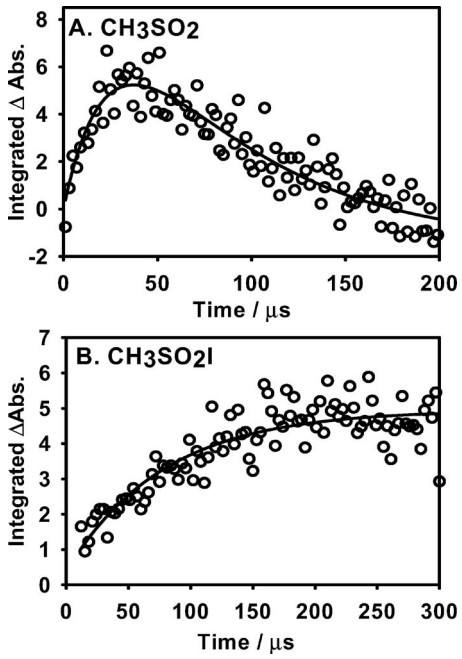

FIG. 8. Temporal profiles of the A1 absorption band of CH_3SO_2 integrated over 1280–1300 cm^{-1} (A) and the B1 absorption band of CH_3SO_2I integrated over 1172–1146 cm^{-1} (B) recorded upon 248 nm photolysis of a flowing mixture of $CH_3I/SO_2/CO_2$ (1.0/3.3/200) at 298 K and 297 Torr. Fitted results are represented with solid lines; see text.

model with first-order rise (k_1^I) and decay (k_{1d}^I) yields $k_1^I = (4.0\pm0.6)\times10^4\ s^{-1}$ and $k_{1d}^I = (1.2\pm0.2)\times10^4\ s^{-1}$, respectively.

The rise is associated with the reaction

$$CH_3 + SO_2 + M \rightarrow CH_3SO_2 + M, \quad (1)$$

whereas the decay might be associated mainly with the reaction

$$CH_3SO_2 + I + M \rightarrow CH_3SO_2I + M. \quad (2)$$

Dividing the value of k_1^I with $[SO_2]=1.55\times10^{17}$ molecule cm^{-3} yields the bimolecular reaction coefficient $k_1^{II}=(2.6\pm0.5)\times10^{-13}$ cm^3 molecule^{-1} s^{-1}. The literature value for the high-pressure limit of k_1 is $(2.9\pm0.5)\times10^{-13}$ cm^3 molecule^{-1} s^{-1},[47] consistent with our observation.

The temporal profile of the B1 band was fitted with a single-exponential rise, shown in Fig. 8(B), to yield $k_2^I = (1.3\pm0.2)\times10^4\ s^{-1}$; the value is similar to k_{1d}^I, supporting that the formation of CH_3SO_2I resulted from the reaction of CH_3SO_2. Although detailed reaction modeling is unlikely because only limited species were observed in this work, we consider that the proposed mechanism is plausible.

V. CONCLUSION

We employed the step-scan time-resolved Fourier-transform absorption technique to detect the SO_2-symmetric and SO_2-antisymmetric stretching bands of the transient species CH_3SO_2 upon photolysis of a flowing gaseous mixture containing CH_3I, SO_2, and CO_2 with the B3P86/aug-cc-pVTZ method; observed vibrational wave numbers of 1076 and 1280 cm^{-1} and relative IR intensities are consistent with those predicted for the SO_2-symmetric and SO_2-antisymmetric stretching modes of CH_3SO_2, respectively. Our spectra conform satisfactorily to a simulation based on rotational parameters derived from these quantum-chemical calculations. A band near 1159 cm^{-1} might be assigned to the SO_2-symmetric stretching mode of CH_3SO_2I that was produced at a later stage of the reaction. The temporal profile of absorption bands of CH_3SO_2 and CH_3SO_2I provide kinetic information that is consistent with existing data and our proposed mechanism.

ACKNOWLEDGMENTS

We thank V. Stakhursky and T. A. Miller for providing the SPECVIEW software for spectral simulation. National Science Council of Taiwan (Grant No. NSC94-2113-M-009-017) and National Chiao Tung University supported this work.

[1] T. S. Bates, B. K. Lamb, A. Guenther, J. Dignon, and R. E. Stoiber, J. Atmos. Chem. **14**, 315 (1992).
[2] R. J. Charlson, J. E. Lovelock, M. O. Andreae, and S. G. Warren, Nature (London) **326**, 655 (1987).
[3] S. B. Barone, A. A. Turnipseed, and A. R. Ravishankara, Faraday Discuss. **100**, 39 (1995).
[4] D. Borissenko, A. Kukui, G. Laverdet, and G. Le Bras, J. Phys. Chem. A **107**, 1155 (2003).
[5] A. Kukui, V. Bossoutrot, G. Laverdet, and G. Le Bras, J. Phys. Chem. A **104**, 935 (2000).

[6] A. Ray, I. Vassalli, G. Laverdet, and G. Le Bras, J. Phys. Chem. **100**, 8895 (1996).
[7] N. R. Jensen, J. Hjorth, C. Lohse, H. Skov, and G. Restelll, J. Atmos. Chem. **14**, 95 (1992).
[8] A. A. Turnipseed, S. B. Barone, and A. R. Ravishankara, J. Phys. Chem. **96**, 7502 (1992).
[9] S. P. Urbanski, R. E. Stickel, and P. H. Wine, J. Phys. Chem. A **102**, 10522 (1998).
[10] V. Riffault, Y. Bedjanian, and G. Le Bras, J. Phys. Chem. A **107**, 5404 (2003).
[11] T. E. Eriksen and J. Lind, Radiochem. Radioanal. Lett. **25**, 11 (1976).
[12] C. Chatgilialoglu, D. Griller, and M. Guerra, J. Phys. Chem. **91**, 3747 (1987).
[13] A. G. Davies, B. P. Roberts, and B. R. Sanderson, J. Chem. Soc., Perkin Trans. 2 **1973**, 626.
[14] C. Chatgilialoglu, B. C. Gilbert, C. M. Kirk, and R. O. C. Norman, J. Chem. Soc., Perkin Trans. 2 **1979**, 1084.
[15] M. D. Sevilla, D. Becker, and M. Yan, Int. J. Radiat. Biol. **57**, 65 (1990).
[16] C. Chatgilialoglu, B. C. Gilbert, and R. O. C. Norman, J. Chem. Soc., Perkin Trans. 2 **1980**, 1429.
[17] A. J. Frank and F. Turecek, J. Phys. Chem. A **103**, 5348 (1999).
[18] R. J. Boyd, A. Gupta, R. F. Langler, S. P. Lownie, and J. A. Pincock, Can. J. Chem. **58**, 331 (1980).
[19] S. R. Davis, J. Phys. Chem. **97**, 7535 (1993).
[20] M. L. McKee, Chem. Phys. Lett. **211**, 643 (1993).
[21] S. M. Resende and F. R. Ornellas, J. Braz. Chem. Soc. **13**, 565 (2002).
[22] S.-H. Chen, L.-K. Chu, Y.-J. Chen, I-C. Chen, and Y.-P. Lee, Chem. Phys. Lett. **333**, 365 (2001).
[23] L.-K. Chu, Y.-P. Lee, and E. Y. Jiang, J. Chem. Phys. **120**, 3179 (2004).
[24] J. Eberhard, P.-S. Yeh, and Y.-P. Lee, J. Chem. Phys. **107**, 6499 (1997).
[25] Y.-J. Chen, L.-K. Chu, S.-R. Lin, and Y.-P. Lee, J. Chem. Phys. **115**, 6513 (2001).
[26] E. Y. Jiang, Spectroscopy (Eugene, Or.) **17**, 22 (2002).
[27] W. Uhmann, A. Becker, C. Taran, and F. Siebert, Appl. Spectrosc. **45**, 390 (1991).
[28] O. V. Rattigan, D. E. Shallcross, and R. A. Cox, J. Chem. Soc., Faraday Trans. **93**, 2839 (1997).
[29] M. J. Frisch, G. W. Trucks, H. B. Schlegel *et al.*, GAUSSIAN 03 Revision A.7, Gaussian Inc., Pittsburgh, PA, 2003.
[30] A. D. Becke, J. Chem. Phys. **98**, 5648 (1993).
[31] C. Lee, W. Yang, and R. G. Parr, Phys. Rev. B **37**, 785 (1988).
[32] J. P. Perdew, Phys. Rev. B **33**, 8822 (1986).
[33] T. H. Dunning, Jr., J. Chem. Phys. **90**, 1007 (1989).
[34] D. E. Woon and T. H. Dunning, Jr., J. Chem. Phys. **98**, 1358 (1993).
[35] M. H. Sirvetz, J. Chem. Phys. **19**, 938 (1951).
[36] K. P. Huber and G. Herzberg, *Constants of Diatomic Molecules*, Molecular Spectra and Molecular Structure IV (Van Nostrand Reinhold, New York, 1979).
[37] R. W. Kilb, J. Chem. Phys. **23**, 1736 (1955).
[38] M. Bahou, S.-F. Chen, and Y.-P. Lee, J. Phys. Chem. A **104**, 3613 (2000).
[39] R. R. Williams, Jr. and R. A. Ogg, Jr., J. Chem. Phys. **15**, 696 (1947).
[40] K. Bogumil, J. Orphal, T. Homann *et al.*, J. Photochem. Photobiol., A **157**, 167 (2003).
[41] W. B. DeMore, S. P. Sander, D. M. Golden, R. F. Hampson, M. J. Kurylo, C. J. Howard, A. R. Ravishankara, C. E. Kolb, and M. J. Molina, *Chemical Kinetics and Photochemical Data for Use in Stratospheric Modeling* (Jet Propulsion Laboratory, Pasadena, CA, 1997).
[42] L. S. Rothman, C. P. Rinsland, A. Goldman *et al.*, J. Quant. Spectrosc. Radiat. Transf. **60**, 665 (1998).
[43] V. Stakhursky and T. A. Miller, 56th OSU International Symposium on Molecular Spectroscopy, Columbus, OH, 2001 SpecView: Simulation and Fitting of Rotational Structure of Electronic and Vibronic Bands, http://www.chemistry.ohio-state.edu/~vstakhur
[44] NIST/EPA Gas-Phase Infrared Database, NIST Standard Reference Database 35, U.S. Department of Commerce, National Institute of Standards and Technology, Gaithersburg, MD, 2004.
[45] G. Geiseler and B. Nagel, J. Mol. Struct. **16**, 79 (1973).
[46] B. Ballesteros, N. R. Jensen, and J. Hjorth, J. Atmos. Chem. **43**, 135 (2002).
[47] F. C. James, J. A. Kerr, and J. P. Simons, J. Chem. Soc., Faraday Trans. 1 **69**, 2124 (1973).